RSC Advances

ROYAL SOCIETY OF CHEMISTRY

www.rsc.org/advances

RSC Advances

RSCPublishing

ARTICLE

Graphene film growth on sputtered thin Cu-Ni alloy film by inductively coupled plasma chemical vapor deposition

Cite this: DOI: 10.1039/x0xx00000x

Received 00th January 2014,
Accepted 00th January 2014

DOI: 10.1039/x0xx00000x

www.rsc.org/

Eunho Kim [a,b], Yong Seung Kim[a,c], Jaehyun Park [a,b], Sajjad Hussain[a,b], , Seung-Hyun Chun [a,c], Seong Jun Kim [d], Ki-Seok An [d], Won-Jun Lee [b], Wan-Gyu Lee [e*] and Jongwan Jung [a,b*]

Graphene film growth on Cu-Ni alloy thin film with variant alloy compositions is reported in this paper. A magnetron co-sputtered thin film was applied to precisely vary the alloy composition, and graphene film was grown at conventional growth conditions by inductively coupled plasma chemical vapor deposition. A highly uniform single-layer graphene, mostly bilayer graphene with ~ 70% coverage, and mostly few-layer graphene were obtained on the Cu-Ni alloys with 8.6, 21, and 34.8 atom % Ni, respectively. The measured resistance decreased from ~1429Ω/sq, to ~756Ω/sq and to ~240Ω/sq, and the transmittance decreased from 97%, to 95% and to 89%, respectively, as the Ni composition increased. The film thickness of graphene layers could be controllable by tuning the alloy composition via the co-sputtering process. But the analysis also indicates that, at the same time, the degree of disordered stacking between layers also tends to increase with increasing Ni content in the Cu-Ni film.

Introduction

Graphene is a one-atom thick sheet of carbon atoms wherein the carbon atoms are arranged in a 2-D hexagonal lattice.[1-3] Graphene has extraordinary electronic properties, including a high electron mobility, which could lead to super-fast transistors and ultra-thin and/or transparent conductors. Electrical properties of graphene change with the number of layers.[4-6] Unlike single-layer graphene (SLG), bilayer graphene (BLG) has a continuous tunable bandgap under an electric field [7] that is useful for electronic devices. And few-layer graphene (FLG) is favorable for the application of transparent electrodes since low sheet resistance is required. Therefore, controllable growth of graphene film is a basic requirement to fully utilize the unique properties of graphene material for practical applications. A promising technique for producing graphene is chemical vapor deposition (CVD) wherein the metal catalyst is exposed to a gaseous hydrocarbon source at an elevated temperature on polycrystalline metal catalysts. [8-14] Among them, copper (Cu) and nickel (Ni) are the most common catalysts. Due to little carbon solubility in Cu, which is less than 0.001 atom % (at %)[15,16] at 1000 ^{o}C, SLG is preferentially formed on Cu (especially in low pressure CVD growth conditions).[11] On the contrary, FLG is more likely to be grown on Ni due to its relatively high carbon solubility (~1.3 at % of carbon at 1000 ^{o}C). [11,17,18] Because Cu-Ni is a well-known binary isomorphous system, Cu-Ni alloy would be an ideal substrate, providing tunable carbon solubility by adjusting the atomic fraction of alloy. The employment of Cu-Ni alloy for graphene growth has been recently reported. S.Chen *et al.* firstly reported CVD-grown BLG with about 70% coverage using a commercial 70:30 Cu-Ni alloy foil.[18] A thick graphite film was grown at relatively a low cooling rate (5 ^{o}C/s), whereas SLG to BLG was obtained only at an exceptionally high cooling rate (~100 ^{o}C/s), which is very difficult to control in large scale production. Most recently, D. Wan *et al.* [19] used a Ni-coated Cu foil. They showed that as growth temperature decreases, the Ni content at the surface of substrate increases, and in turn the layer number of graphene increases. BLG was obtained at a relatively low temperature of 850 ^{o}C, and three-layer graphene and five-layer graphene at much lower temperatures of 750 ^{o}C, and 650 ^{o}C, respectively. But there is concern about the poor crystalline quality of CVD-grown graphene at such a low temperature even though lowering the growth temperature is desirable.

In this paper, a magnetron co-sputtered thin film was applied to precisely vary the composition of Cu-Ni alloy (8.6, 21, 34.8 Ni at %), and graphene was grown under conventional CVD growth conditions (at conventional cooling rate, ~3^{o}C/min and growth temperature, 950^{o}C). We investigated the layer thickness controllability and qualities of CVD-grown graphene film.

Experimental

As a thin metal catalyst, 600~800 nm- thick Cu-Ni alloy films were deposited by magnetron co-sputtering (1.5~2.5kW, 10 mTorr, Ar 100 sccm) on 8 inch- 300 nm-SiO_2/Si substrates. The alloy compositions of thin films were confirmed by inductively coupled plasma mass spectrometer (ICP-MS) and X-ray photoelectron spectroscopy (XPS). The wafers were then broken into pieces, and the metal-deposited substrates (1-2 cm^2 in size) were loaded into a radio frequency (RF) CVD system with a cold-wall chamber.[20] The chamber was equipped with an inductively coupled plasma (ICP)

reactor and pumped with a turbomolecular pump, keeping the base pressure as low as ~10^{-7} torr. [20] The substrates were heated to the growth temperature without any gas flow into the chamber. When it reached the target temperature, hydrogen gas was injected into the chamber at the flow rate of 40 sccm. Hydrogen gas was discharged by an RF power of 50 W for 2 min to eliminate surface oxides on the Cu-Ni alloy film. Graphene films were grown at 100 W RF power, Ar:CH_4=50:2sccm flow rate, and 20 mTorr pressure for 10 sec. Subsequently, we turned off the silicon carbide (SiC) heater to cool down the samples to room temperature. The cooling rate at a high temperature, ranged from 950 to 600 ^oC, is observed as ~3 ^oC/min approximately. After CVD synthesis was done, the graphene film was released by protecting the graphene sheets with poly(methylmethacrylate) (PMMA) and etching the underlying metal catalyst with HCl and $FeCl_3$. Once the PMMA/graphene film was transferred onto the target substrate, the PMMA was removed by acetone. The synthesized graphene films were characterized by optical microscope, scanning electron microscope (SEM), transmission electron microscopy (TEM), Raman spectroscopy, and four- point probe measurement.

Results and discussion

Table.1 shows the at % of Cu and Ni in Cu-Ni alloys measured by ICP-MS. The at % of Ni was confirmed as 8.6, 21, 34.8 for the three samples (G1, G2 and G3 samples, respectively). The at % in the alloy film was also confirmed uniform by XPS. Figure 1 shows optical microscope images of graphene films transferred to 300 nm SiO_2/Si substrates. The optical image suggests that Cu-Ni alloys with lower Ni contents produce thinner and more uniform graphene films. Raman spectroscopy and optical contrast analysis were used to determine the thickness of the graphene layers. To avoid the ambiguity of Raman analysis in determining the number of graphene layers, optical contrast analysis was employed. When graphene film is placed on the substrate, it creates an enhanced absorption at a wavelength of around 550 nm, corresponding to the color green.[21,22] Each green values of each pixel (1376 by 10381,428,288 pixels) of G1-G3 samples were extracted on a scale of 8 bits (0-255). Furthermore, the relative difference between the green value of each pixel and that of a bare SiO_2/Si substrate, ΔG, was calculated. As the number of graphene layers increases, green intensity due to absorption decreases, thus the ΔG increases. Distribution of ΔG was statistically analysed to see the uniformity of graphene thickness. By characterizing the green color contrast of the graphene layers with respect to the underlying SiO_2/Si in the optical microscope image, the layer thickness can be obtained. [23] Figure 1(d) shows that the G1 sample with 8.6% Ni composition exhibits mostly SLG; the G2 sample with 21% Ni composition exhibits BLG with a coverage of around 70% coverage; and, the G3 sample with 34.8% exhibits mostly FLG (3L+). The produced graphene film becomes thicker from SLG to BLG and to FLG through tuning the Ni composition from 8.6, to 21 and to 34.8%. In order to investigate the quality and degree of interlayer stacking of graphene layers, micro-Raman spectroscopy (Renishaw invia RE04, 514nm Ar laser) was used, and Raman mapping was taken over a 30×30μm^2 area. The mapped Raman spectra of G1 sample are shown in Fig. 2(a,b,c). The mapped 2D bands exhibit mostly single Lorentzian profiles with ~ 39±2.2 cm^{-1} full width at half maximum (FWHM), ~2688 ±4 cm^{-1} peak position, and a ratio of 2D to G peak intensities (I_{2D}/I_G) of ~2.5±0.2. The D band, a marker of disorder-induced defects is quite small as shown in the representative Raman spectra in Fig.3(a). Those Raman data suggest that uniform and high-quality SLG was grown over the G1 sample.

Table 1. Atomic % of Cu and Ni in Cu-Ni alloys measured by ICP-MS.

	Cu(μg)	Ni(μg)	Cu:Ni
G1	382	35.9	91.4:8.6 (%)
G2	413	110	79:21 (%)
G3	141	75.3	65.2:34.8 (%)

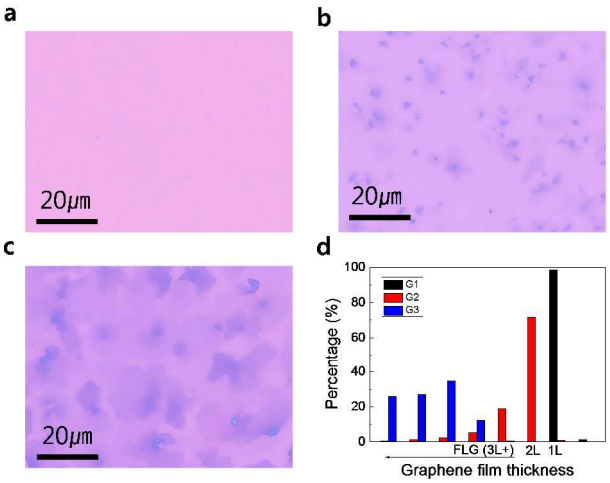

Fig.1. Optical images of graphene films transferred after grown on (a) 8.6% at % Ni (G1), (b) 21 % Ni (G2) , and (c) 34.8% Ni (G3) in Cu-Ni alloys. (d) Thickness distribution of graphene films for three samples, measured by optical contrast.

The mapped 2D bands of the G2 sample exhibit FWHM of ~50±9.2cm^{-1}, peak position at ~2700±3cm^{-1}, and I_{2D}/I_G of ~1.1±0.8. It can be seen that the 2D band became broader and blue-shifted. And the mapping Raman spectra of G2 samples show less uniform distribution than those of the G1 sample (Fig.2(d,e)).

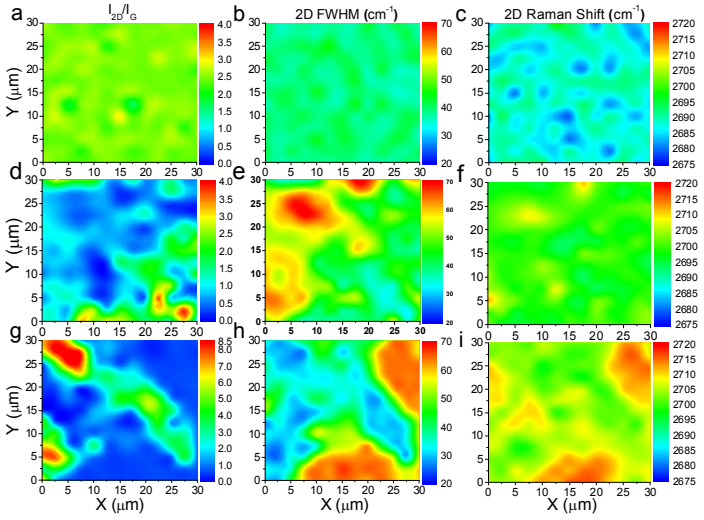

Fig.2 Raman mapping measurements of graphene films for (a,b,c) G1, (d,e,f) G2, and (g,h,i) G3 samples. Shown in the figures are the color-coded intensity mapping of I_{2D}/I_G (a,d,g), 2D FWHM (b,e,h), and 2D shift (c,f,i) over 30 μm × 30 μm area.

It was noted that I_{2D}/I_G and 2D FWHM show different values even on the same graphene layer thickness (exhibiting the same optical contrast), which suggests that the degree of interlayer stacking is not uniform over the G2 sample. A middle Raman spectrum in Fig.3(b)

exhibits AB-stacked or low-angle misoriented BLG. Turbostratic (high-angle misoriented) BLG was also spotted (top one of Fig.3(b), 2D FWHM of ~32 and I_{2D}/I_G of ~3).

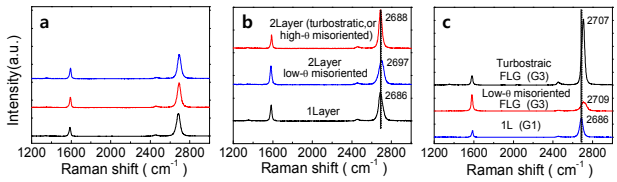

Fig.3 Some representative Raman spectra of (a) G1, (b) G2, and (c) G3 samples.

The Raman spectra of BLG strongly depend on the relative orientation of each layer.[24, 25] Low-angle (< ~8°) misoriented BLG exhibits the Raman signature of strong coupling between layers. On the contrary, in the high angle regime (> 13°), the BLG displays Raman spectra closer to those of SLG. [25] Figs.4(a) and (b) show a histogram of I_{2D}/I_G and 2D FWHM of G2 sample.

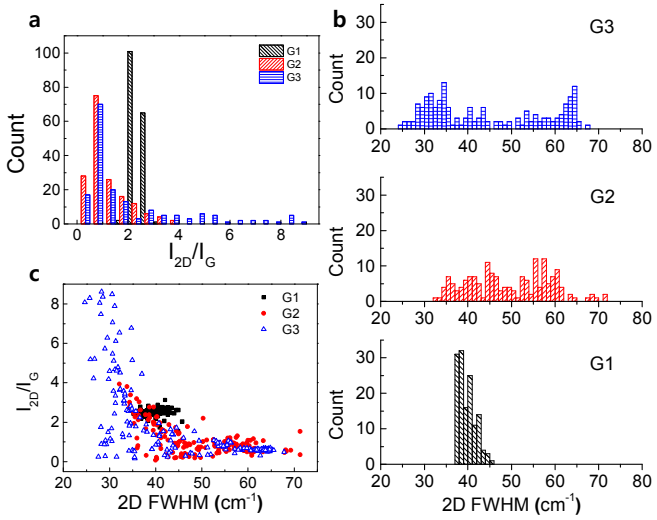

Fig.4 Histogram distribution of (a) I_{2D}/I_G and (b) 2D FWHM, and (c) I_{2D}/I_G versus 2D FWHM plot.

The turbostratic BLG has a very narrow 2D band down to 32 cm^{-1} and very high I_{2D}/I_G up to 4. It is noted that the 2D peak is similar but sharper and more intense than that of SLG. As shown in the histogram of 2D FWHM (Fig.4(a)) and 2D FWHM versus I_{2D}/I_G curve (Fig.4(c)), there are some distribution portions that exhibit low 2D FWHM (or high I_{2D}/I_G), in which BLG is misoriented in high angle. Fig. 5(a) shows I_{2D}/I_G versus ratio of 2D to G integral intensities (A_{2D}/A_G). It can be seen that there are also some distribution portions showing sharper 2D peaks at the same I_{2D}/I_G ratios, which are most likely to be high angle misoriented BLG. These results suggest that AB stacked or low-angle misoriented BLG coexists with turbostratic BLG (high-angle misoriented) over the G2 film. The mapped 2D bands of the G3 sample seem to exhibit more non-uniform distribution than the G2 sample. Like the G2 sample, stacked and turbostratic FLG are mixed over the G3 sample. Turbostratic FLG has very broad range of I_{2D}/I_G up to ~8.7 (Fig.4(a)) due to different degrees and the order of misorientation between layers.

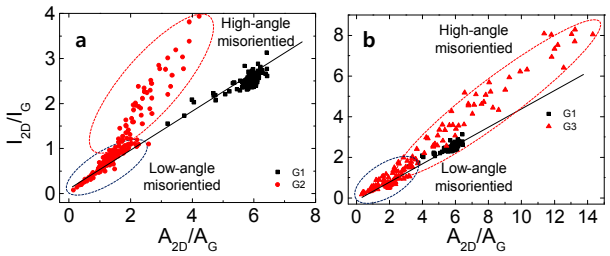

Fig.5 I_{2D}/I_G versus ratio of 2D to G integral intensities (A_{2D}/A_G).

The degree of interlayer staking could be further inferred in the histogram of 2D FWHM (Fig.4(b)), 2D FWHM versus I_{2D}/I_G curve (Fig.4(c)), and I_{2D}/I_G versus A_{2D}/A_G curve (Fig.5(b)). There is a significant portion exhibiting very low 2D FWHM (even much lower than that of SLG) or very high I_{2D}/I_G (much higher than that of SLG), in which FLG is misoriented in high angle. From the above Raman analysis, it can be concluded that as the Ni content increases in the Cu-Ni alloy film, graphene film grows thicker, and at the same time, the degree of disordered stacking between layers also tends to increase. Generally, the turbostratic graphene is due to the dislocations between two graphene layers, [26] and a slower crystal growth rate could yield fewer crystalline dislocations. It is reported that a slow cooling rate (5 °C/min) favors AB-stacked bilayer.[27] Therefore, we think that the possibility of disordered stacking between layers could be more or less mitigated by a slow cooling rate. However, a slow cooling rate also increases the thickness of graphene film and the process time. Please note that a thick graphite film was obtained on 70:30 Cu-Ni alloy foil at low cooling rate. [18] High resolution TEM was also employed to characterize the crystallinity of the graphene films.

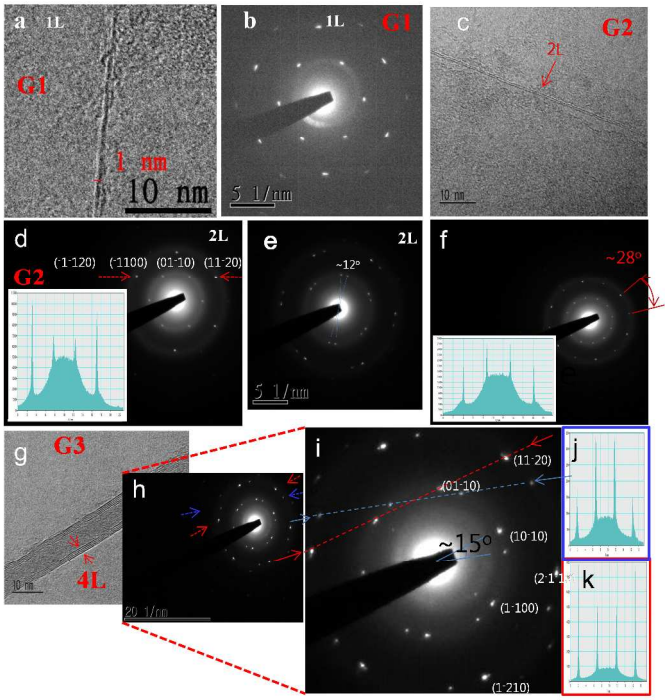

Fig.6 High resolution TEM of grown graphene samples. (a,b) G1, (c-f) G2, and (g-k) G3.

The edges of the monolayer for the G1 sample are clearly seen in the TEM image as in Fig.6(a). Selected-area electron diffraction (SAED) patterns for SLG are shown in Fig.6(b). In Fig.6(c), bilayer (2L) is clearly seen at the folded edges of the G2 sample. Figs.6 d-f show

SAED patterns taken at different regions of the G2 sample and its diffraction intensities. In Fig.6(d), only one set of diffraction patterns with 6-fold symmetry is found. The intensity of the first-order diffraction is lower than that of the second order, indicating that the bilayer graphene in this region is Bernal stacked.[28,29] On the contrary, SAED pattern of Fig.6(e) shows a rotation angle of ~ 12º between two layers, and Fig.6(f) shows a high rotation angle of ~ 28º between two layers. It can be also seen that the intensity of the first-order diffraction is higher than that of the second order. Thus, it can be confirmed that Bernal stacking and low to high angle misorientation of bilayer co-exist in sample G2. In Fig.6(g), four-layer (4L) is seen at the folded edge of the G3 sample. Fig.6(h) displays SAED patterns for the G3 sample. Intensity of the diffraction spots along the blue and red lines are shown in Fig.6(j) and (k), respectively. In k, the intensity of the first-order diffraction is lower than that of the second order, indicating Bernal stacking; and in j, the intensity of the first-order diffraction is higher than that of the second order, indicating one more layer is stacked. In the enlarged diffraction patterns, j, an additional diffraction spot can be found with only a slight rotation by 1°. Thus, it can be concluded that the four layers are stacked in this region, in which two layers are Bernal stacked, one layer is low-angle misoriented (~1º), and one layer is high-angle misoriented with ~15º. It was a lengthy process to discover Bernal stacking in the G3 sample. Thus, TEM analysis supports that as Ni content in Cu-Ni alloy increases, interlayer disorder of synthesized CVD-graphene also tends to increases. Optical and electrical properties were measured using graphene films transferred to a glass substrate. To the naked eye, the graphene samples exhibit decreasing transmittance from G1 to G3 sample. As shown in Fig. 7(b), the G1 sample has a transmittance of 96.1% at 550 nm. Such values are close to ~ 97%,[30] the optical transparency of SLG, implying that the G1 sample is predominantly monolayer. The slight difference in the value is attributed to the coverage of graphene domains and wrinkles, and defects in the transferred films. The G2 sample has transmittance of 95% at 550 nm, indicating mostly BLG. The G3 sample has a transmittance of 89%, consistent with ~ 4~5 layers. The optical transmittance data coincide well with the previous analysis of Raman spectra and optical contrast data.

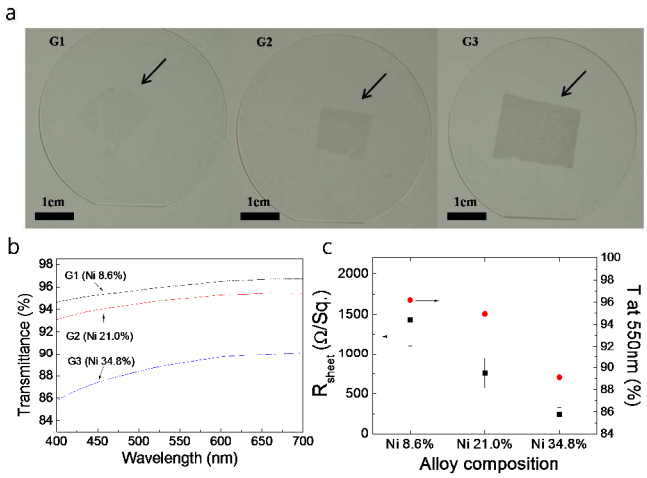

Fig.7 (a) Optical images of graphene films transferred on quartz substrate. (b) Optical transmittance of graphene films. (c) Electrical sheet resistance and optical transmittance value at 550 nm with respect to the Ni contents of Cu-Ni alloy films.

The sheet resistance, Rs, was measured by the van der Pauw method. The G1, G2, and G3 samples have ~1429 Ω/sq, ~756Ω/sq, and ~240Ω/sq, respectively. The average sheet resistance decrease with the layer thickness, as expected. Fig.7 (c) summarizes the sheet resistance and transmittance values for all samples.

Conclusions

We reported graphene film growth on Cu-Ni alloy thin film with variant alloy compositions (8.6, 21, and 34.8 at % Ni). Cu-Ni alloy film was prepared by a co-sputtering process, and graphene was grown at conventionally high temperature and normal cooling rate by ICP-CVD. Highly uniform SLG, mostly BLG with ~ 70% coverage and mostly FLG (~3+), were obtained on Cu-Ni alloys with 8.6, 21, and 34.8 at % Ni, respectively. The measured resistance decreased from ~1429 Ω/sq, to 756 Ω/sq and to ~240 Ω/sq as the Ni composition increases. And the transmittance also decreased from 97%, to 95% and to 89%. As the Ni content increases in the Cu-Ni alloy film, the thickness of CVD-graphene film also increases. On the other hand, Raman mapping and TEM analysis also indicated that, at the same time, the degree of disordered stacking between layers also tends to increase with increasing Ni content in Cu-Ni alloy.

Acknowledgements

This research was supported by the Technology Innovation Program (industrial strategic technology development program,10035430, development of reliable fine-pitch metallization technologies) funded by the Ministry of Knowledge Economy (MKE, Korea).

Notes and references

[a] Graphene Research Institute, Sejong University, Seoul 143-747, Korea
[b] Institute of Nano and Advanced Materials, Sejong University, Seoul 143-747, Korea
[c] Department of Physics, Sejong University, Seoul 143-747, Korea
[d] Thin Film Materials Research Group, Korea Research Institute of Chemical Technology, Daejon 305-600, Korea
[e] Department of Nanodevice, National NanoFab Center, Daejeon, Korea

† Corresponding authors, E-mail: jwjung@sejong.ac.kr, wangyulee@nnfc.com

1 Novoselov KS, Geim AK, Morozov SV, Jiang D, Zhang Y, Dubonos SV, et al., Science, 2004, 306, 666.
2 Balandin AA, Ghosh S, Bao WZ, Calizo I, Teweldebrhan D, Miao F, et al., Nano Lett., 2008, 8,902.
3 Bonaccorso F, Sun Z, Hasan T, Ferrari AC. Graphene photonics and optoelectronics. Nat Photonics, 2010,4,611.
4 Rana F, IEEE T Nanotechnol, 2008,7,91.
5 Liu M, Yin XB, Ulin-Avila E, Geng BS, Zentgraf T, Ju L, et al., Nature, 2011,474,64.
6 Liu N, Liu H, Zhu SN, Giessen H. Nat Photonics, 2009,3,157.
7 Samarakoon DK, Wang XQ., Acs Nano, 2010,4,4126.
8 Coraux J, N'Diaye AT, Busse C, Michely T, Nano Lett., 2008,8,565.
9 Sutter PW, Flege JI, Sutter EA, Nat Mater., 2008,7,406.
10 Reina A, Jia XT, Ho J, Nezich D, Son HB, Bulovic V, et al., Nano Lett., 2009,9,30.
11 Li XS, Cai WW, Colombo L, Ruoff RS., Nano Lett., 2009,9,4268.
12 Kim E, An H, Jang H, Cho WJ, Lee N, Lee WG, et al., Chem Vapor Depos, 2011,17,9.
13 An H, Lee WJ, Jung J., Curr Appl Phys, 2011,11,S81.
14 An H, Lee WG, Jung J., Curr Appl Phys, 2012,12,1113.
15 Mathieu G, Guiot S, Cabane J., Scripta Mater, 1973,7,421.

16 Lopez GA, Mittemeijer E., Scripta Mater, 2004,51,1.
17 Cai WW, Piner RD, Zhu YW, Li XS, Tan ZB, Floresca HC, et al., Nano Res, 2009,2,851.
18 Chen SS, Cai WW, Piner RD, Suk JW, Wu YP, Ren YJ, et al., Nano Lett., 2011,11,3519.
19 Wan DY, Lin TQ, Bi H, Huang FQ, Xie XM, Chen IW, et al., Adv Funct Mater, 2012,22,1033.
20 Kim YS, Lee JH, Kim YD, Jerng SK, Joo K, Kim E, et al., Nanoscale 2013,5,1221.
21 Blake P, Hill EW, Neto AHC, Novoselov KS, Jiang D, Yang R, et al., Appl Phys Lett., 2007,91.
22 Roddaro S, Pingue P, Piazza V, Pellegrini V, Beltram F., Nano Lett., 2007,7,2707.
23 Reina A, Thiele S, Jia XT, Bhaviripudi S, Dresselhaus MS, Schaefer JA, et al., Nano Res, 2009,2,509.
24 Luo ZQ, Yu T, Shang JZ, Wang YY, Lim S, Liu L, et al., Adv Funct Mater, 2011,21,911.
25 Kim K, Coh S, Tan LZ, Regan W, Yuk JM, Chatterjee E, et al., Phys Rev Lett., 2012,108.
26 Robertson AW, Bachmatiuk A, Wu YMA, Schaffel F, Rellinghaus B, Buchner B, et al., Acs Nano, 2011,5,6610.
27 Wu YP, Chou H, Ji HX, Wu QZ, Chen SS, Jiang W, et al. , Acs Nano, 2012,6,7731.
28 A. C. Ferrari, J. C. Meyer, V. Scardaci, C. Casiraghi, M. Lazzeri, F. Mauri, S. Piscanec, D. Jiang, K. S. Novoselov, S. Roth and A. K. Geim, *Phys Rev Lett*, 2006, 97.
29 J. C. Meyer, A. K. Geim, M. I. Katsnelson, K. S. Novoselov, T. J. Booth and S. Roth, *Nature*, 2007, 446, 60-63.
30 Nair RR, Blake P, Grigorenko AN, Novoselov KS, Booth TJ, Stauber T, et al., Science, 2008,320,1308.